RSC Advances

REVIEW

View Article Online
View Journal | View Issue

Cite this: *RSC Adv.*, 2021, **11**, 6628

Aligned carbon nanotube fibers for fiber-shaped solar cells, supercapacitors and batteries

Yufang Cao,[abc] Tao Zhou,[c] Kunjie Wu, *[bc] Zhenzhong Yong*[bc] and Yongyi Zhang[abc]

Aligned carbon nanotube (CNT) fibers have been considered as one of the ideal candidate electrodes for fiber-shaped energy harvesting and storage devices, due to their merits of flexibility, lightweight, desirable mechanical property, outstanding electrical conductivity as well as high specific surface area. Herein, the recent advancements on the aligned CNT fibers for energy harvesting and storage devices are reviewed. The synthesis, structure, and properties of aligned carbon nanotube fibers are briefly summarized. Then, their applications in fiber-shaped energy harvesting and storage devices (*i.e.*, solar cells, supercapacitors, and batteries) are demonstrated. The remaining challenges are finally discussed to highlight the future research direction in the development of aligned CNT fibers for fiber-shaped energy devices.

Received 7th November 2020
Accepted 25th January 2021

DOI: 10.1039/d0ra09482j

rsc.li/rsc-advances

1. Introduction

Wearable electronics with miniaturization, intelligence and flexibility have attracted great interest and can be widely used in various fields, bringing great convenience to people's lives.[1–4] Currently, various wearable electronics have been rapidly developed from initial accessories (*i.e.*, smart bracelet, smart watch, Google glasses) to present smart textiles (*i.e.*, smart sportswear, smart high-heels, smart running-socks and so on), which are very attractive for consumers. Accompanied with the rapid growth of wearable devices, matching energy harvesting and storage systems are urgently needed.[5–8] Among a variety of power systems, the fiber-shaped energy devices have been regarded as a promising strategy due to their more outstanding flexibility and knittability than planar-shaped ones, and because they can be easily integrated or directly woven into various textile products with different forms.[9–14] However, there exist several great challenges in fiber-shaped energy devices: (1) the relatively low capacity resulting in the repeated charging; (2) limited mechanical properties (*i.e.*, stretchability, flexibility, foldability, *etc.*) to withstand severe and frequent deformation during usage.

The mechanical and electrochemical performance of fiber-shaped energy device are highly dependent on the electrode properties. Compared with commonly used fiber electrodes, such as metal wire, conductive polymer fiber, and metal coated

[a]*School of Nano-Tech and Nano-Bionics, University of Science and Technology of China, Hefei 230026, Anhui, China*

[b]*Key Laboratory of Multifunctional Nanomaterials and Smart Systems, Advanced Materials Division, Suzhou Institute of Nano-Tech and Nano-Bionics, Chinese Academy of Sciences, Suzhou 215123, Jiangsu, China. E-mail: kjwu2014@sinano.ac.cn; zzyong2008@sinano.ac.cn*

[c]*Division of Nanomaterials, Jiangxi Key Lab of Carbonene Materials, Suzhou Institute of Nano-Tech and Nano-Bionics, Nanchang, Chinese Academy of Sciences, Nanchang 330200, Jiangxi, China*

Yufang Cao is a PhD student in the School of Nano-Tech and Nano-Bionics, University of Science and Technology of China, working under the supervision of Dr, Professor Yongyi Zhang. She received her BTech in CAS Key Laboratory of Carbon Materials, Institute of Coal Chemistry, China in 2018. Her current research focuses on the development of carbon nanotube composites for energy storage devices.

Tao Zhou received his MA degree in Materials Chemistry at Jiangxi Science & Technology Normal University in 2018, afterwards working at Division of Nanomaterials, Suzhou Institute of Nano-tech and Nano-bionics, Nanchang (SINANONC), Chinese Academy of Sciences. His current research focuses on the continuous fabrication and strengthening of carbon nanotube fibers.

artificial/natural fiber, aligned carbon nanotube (CNT) fibers have been considered as promising electrodes for fiber-shaped energy harvesting and storage devices due to its merits of lightweight, desirable mechanical properties (*i.e.*, high strength and flexibility), outstanding electrical conductivities as well as high specific surface area.[15–17] Up to now, a lot of efforts have been made to explore the applications of aligned CNT fibers as charge collector, effective supporter for active nanoparticles, and reactive interface for electrochemical processes in fiber-shaped energy devices. In this review, the fabrication and fundamental properties of aligned CNT fibers are briefly summarized. Then, their applications in fiber-shaped energy harvesting (*i.e.*, fiber-shaped solar cells) and storage (*i.e.*, supercapacitors and lithium-ion batteries) devices are described. Finally, the remaining challenges will be discussed to highlight the future direction in the development of aligned CNT fibers for enhanced fiber-shaped energy devices.

2. The synthesis and fundamental properties of aligned CNT fibers

Aligned CNT fiber is a typical macroscopic material assembled from numerous carbon nanotubes. The mechanical and electrical properties of aligned CNT fiber are highly dependent on the spinning methods, which will greatly affect the mechanical and electrochemical performance of fiber-shaped energy devices. Excellent conductivity of aligned CNT fiber is favorable to the fast charge transport, and its outstanding mechanical properties can ensure the structure stability of fiber energy devices under various severe deformation. The following section briefly describes synthesis and fundamental structural properties of the aligned CNT fibers.

2.1 The synthesis of aligned CNT fibers

Typically, aligned CNT fibers can be fabricated by wet or dry spinning method. For wet spinning, the aligned CNT fibers are obtained from CNT solution dissolved with the assistance of surfactants, strong acids, and polymers, as shown in Fig. 1a.[18] Although the diameters of aligned CNT fibers can be easily controlled, ranging from several to hundreds of micrometers by tuning the processing parameters, it is difficult to continuously spin long CNT fiber. Moreover, much surfactant and/or polymer remained inside or on the surface of CNT fibers will greatly reduce the electrical conductivity (Fig. 1b), resulting in decreased electrochemical performance of devices.

Dry spinning is another commonly used method to fabricate aligned CNT fibers. The aligned CNT fibers can be spun from CNT sheet[19] or vertically aligned CNT array[20] synthesized by chemical vapor deposition (CVD), as shown in Fig. 1c, d and e, f, respectively. In addition, the aligned CNTs fibers can be also directly spun from partially-aligned CNT aerogel in a growth furnace (Fig. 1g).[21] Without the complicated CNT dispersion and purification, the dry-spun aligned CNTs fibers usually possess large aspect ratio, high electrical conductivities, mechanical performance, and low defect/impurity density. Moreover, adjustable structure and properties of aligned CNT fibers can broaden their application fields for enhanced energy storage and harvesting devices.

Benefiting from high specific surface area of CNT fiber, the CNT–active material composite fiber with high electrochemical activity can be successfully prepared for high performance fiber-shaped energy harvesting and storage devices. It is worth noting that the electronic conductivity and mechanical property of aligned CNT fibers will decrease somewhat after compositing with active substance. Therefore, it is important to balance the

Kunjie Wu is currently a research associate at Advanced Materials Division of Suzhou Institute of Nano-tech and Nano-bionics (SINANO), CAS, since 2017. He received the PhD degree in Materials Physics and Chemistry from the University of Science and Technology of China in 2012. From 2014 to 2017, he was with the SINANO as a Post-Doctoral Fellow. His research focuses on the continuous fabrication and strengthening of carbon nanotube fibers, and related applications.

Dr Zhenzhong Yong received his PhD from Shanghai Institute of Applied Physics, CAS in 2008, and bachelor degree from Shandong University in 2003. Currently, he is a Senior Engineer in Suzhou Institute of Nano-Tech and Nano-Bionics, CAS, whose research interests focus on synthesis and applications of carbon nanotube fibers.

Prof. Yongyi Zhang received his PhD and BS degree from Peking University in 2008 and Beijing Normal University in 2002, respectively. He worked as a post Doc in University of Michigan, Ann Arbor, and University of South Dakota from 2008 to 2011. He joined in Suzhou Institute of Nano-Tech and Nano-Bionics, CAS, in 2011 and currently is a full professor focusing on high-performance carbon nanotube fibers and functionalized graphene fibers.

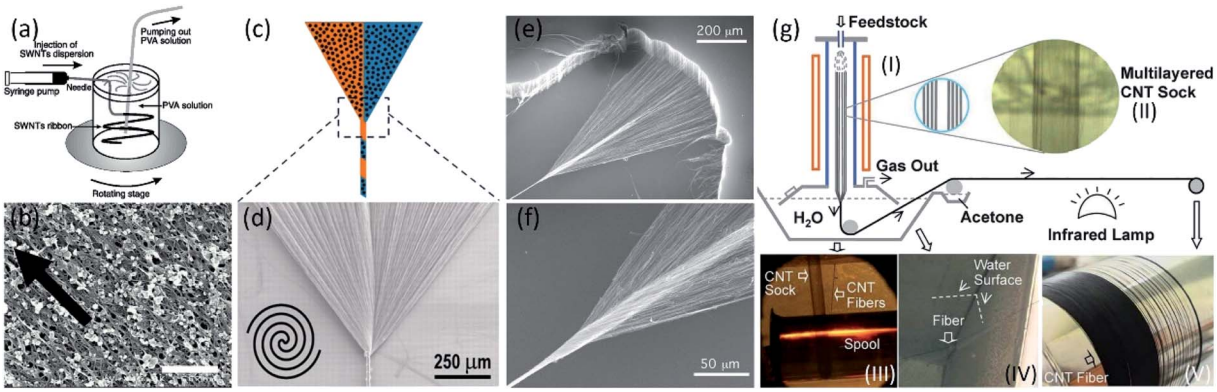

Fig. 1 (a) Schematic of the experimental setup used to make CNT fiber by wet spinning. (b) SEM of the CNT fiber.[18] Copyright 2000, AAAS. (c) Illustration and (d) SEM micrograph of the fabrication of CNT fibers by twisting the CNT sheet.[19] Copyright 2011, AAAS. (e) and (f) SEM images at two different magnifications of a CNT fiber in the process of being simultaneously drawn and twisted during spinning from a CNT forest.[20] Copyright 2004, AAAS. (g) CVD synthesis and spinning set-up for the fabrication of continuous CNT yarns. (I) Schematic diagram of the synthesis and spinning set-up. (II) A photograph showing a layered CNT sock formed in the gas flow. Photographs of the water densification step (III), the drawing of the fiber from the water to the other side of the rotator (IV), and spinning of the finished fiber on the final spool (V).[21] Copyright 2010, Wiley-VCH.

mechanical/physical properties of aligned CNT fibers and the load of active substance.

2.2 Fundamental properties of aligned CNT fibers

The mechanical and electrical properties of aligned CNT fibers make them a good candidate in the wearable and deformable fiber-shaped energy devices with high electrochemical performance, which will be briefly demonstrated in this section. The tensile strength and Young's modulus of aligned CNT fibers are highly dependent on nanotube structures and fiber-processing methods.[22,23] To date, much efforts have been made to strengthen the aligned CNT fibers by stretching,[24,25] physical densification (*i.e.* mechanical pressing or twisting),[26] solvent infiltration–evaporation,[27–30] interface functionalization and *in situ* crosslinking by polymers.[31–36] Up to now, tensile strengths of aligned CNT fibers were ranging from 1 to 10.8 GPa, and the modulus were ranging from 70 to 400 GPa, exhibiting outstanding mechanical properties.[22,37,38] Moreover, aligned CNT fibers also possess superior stretchability and flexibility, which allows the fibers to be bent, twisted, and knotted without obvious structure damage. The superior mechanical properties of aligned CNT fibers can ensure the strength and flexibility for fiber-shaped energy devices, such as solar cells, supercapacitors, and batteries.

Moreover, aligned CNT fibers have the potential to be applied in the next generation high performance energy harvesting and storage devices owing to their superior electrical properties. Similar to the mechanical property, the electrical conductivity of aligned CNT fibers is closely related with nano/micro structures (*i.e.*, alignment, packing density, diameter, length) and preparing processes (*i.e.*, wet-spinning and dry-spinning), varying from several to thousands of S cm^{-1}.[39–42] According to the 3D hopping mechanism, the electrical conductivity is also closely related to the vacancies and structural defects of individual tubes and inter-tube contacts.[40,43] Increasing hopping channels and densifying the assembly are the efficient strategies to enhance the electrical conductivity.

Generally, the vertically-aligned CNT array spun fibers had the relatively low conductivity ($\sim 6 \times 10^4$ S m^{-1}),[44] due to the high percentage of multi-walled CNTs which have more defects than double-walled and single-walled CNTs, and very low packing density. However, the aligned CNTs fibers spun from aerogel and liquid crystals possess more than one order of magnitude larger conductivity (up to 2×10^6 S m^{-1}),[21,45–49] ascribed to the larger fraction of double-walled/single-walled CNTs and higher packing density. Notably, the surfactants and polymeric compounds introduced during wet-spinning process are usually non-conductive, harmful to the conductivity of aligned CNT fibers.[18] So far, acid treatment (HNO_3 treatment),[39] infiltration of conductive particles ($HAuCl_4$ and H_2PtCl_6 ethanol solutions treatment) and physical/chemical doping (iodine doping) have become the major solutions to enhance the conductivity of aligned CNT fibers.[46,50,51]

3. Aligned CNT fibers for energy harvesting and storage devices

Based on the above analysis, aligned CNT fibers have been considered as promising electrodes for fiber-shaped energy harvesting and storage devices due to the extraordinary structural flexibility and stability, desirable mechanical/electrical properties as well as high porosity/surface area. The obtained high-performance CNT-based fiber devices can be easily integrated into the textile by conventional woven techniques for wearable electronics.

3.1 Fiber-shaped solar cells

The photovoltaic properties of fiber-shaped solar cells are highly dependent on the conductive and catalytic properties of fiber electrodes. For conventional fiber-shaped solar cells, conductive metal wires (*i.e.*, Ti wire and Pt wire) are the most commonly used electrode materials due to the high

conductivity and catalytic properties.[52–55] However, its poor flexibility, easy corrosion and heavy weight limit its further development towards wearable fiber-shaped solar cells. Compared with metal wires, aligned CNT fibers are more promising candidate serving as cathode or photoanode for wearable fiber-shaped solar cells, such as dye-sensitized solar cells (DSSCs), polymer solar cells and perovskite solar cells due to their lightweight, flexibility, superior conductivity, high specific surface area and catalytic properties, as listed in Table 1.[14,56] Especially, the high specific surface area is favorable for the physical incorporating or chemical bonding of various active materials (*i.e.*, photo-sensitive dyes, catalytic metal nanoparticles and transition metal oxides) into the aligned CNTs fibers, improving the power conversion efficiency (PCE).

In this regard, the CNT fiber adsorbed with dye molecule (N719) as the working electrode was firstly used to fabricate the dye-sensitized solar cells (DSSCs) coupled with Pt wire as counter electrode.[57] Benefiting from the high conductivity and adsorption capacity of dye molecules of CNT fibers, the obtained DSSCs in planar configuration exhibited a high PCE of 2.2%, which opened up the applications of aligned CNT fibers in fiber-shaped solar cells. Later on, the CNT fiber-based DSSC with twisted structure (Fig. 2a and b) was developed,[58] where the aligned CNT fiber and CNT/PVDF fiber were used as working electrode and counter electrode, respectively. However, the obtained devices showed extremely low PCE of 0.06% (Fig. 2c). This result was mainly ascribed to the low absorption of N719 on surface of CNTs and mismatch of energy levels between N719 and CNTs. To further improve the PCE of the fiber-shaped DSSCs, a random TiO_2 nanocrystal hole blocking layer was introduced into the photovoltaic CNT fiber-based device. After absorption of incident light, the excited dye molecule injects an electron into the conduction band of titanium dioxide, and the electron can rapidly transport along the CNTs. The TiO_2 nanocrystal layer can effectively adsorb more dye molecule to improve photoinduced charge separation and transport of carriers to the electrode. According to the typical *J–V* curve with open-circuit voltage (V_{oc}) of 0.63 V, short-circuit current density (J_{sc}) of 7.72 mA cm^2, and fill factor (FF) of 0.48, the TiO_2-loaded fiber-shaped DSSCs exhibited much higher PCE of 2.32%.[58] Moreover, the performance of aligned CNT fiber-based DSSCs is closely related with photoanode structure. Replacing the random TiO_2-coated CNT fiber, an aligned CNT fiber radially grown with aligned TiO_2 nanotubes was used as photoanode in fiber-shaped DSSCs, which can be more effectively separated along the aligned titanium dioxide nanotubes compared with a lot of interfaces among nanoparticles, resulting in an further enhanced PCE of 3.9% (Fig. 2d).[58] The PCE was also increased to 2.94% by Chen *et al.*, using aligned CNT fiber incorporated with a mesoporous TiO_2 layer as working electrode and bare CNT fiber as counter electrode (Fig. 2e and f). For the working electrode of CNT@TiO_2, the CNT ensure the fast charge transport, and the mesoporous TiO_2 layer here on the CNT fiber favors the dye chemisorption onto the nanoparticle for improved photovoltaic performances.[59] Moreover, benefiting from the outstanding flexibility of aligned CNT fiber, the obtained fiber-shaped devices could be woven into electronic textiles, showing excellent knittability (Fig. 2f inset). Recently, a PCE of 7.39% was achieved by a novel design of core–sheath solid state DSSC by introducing the quantum dots (QDs) (Fig. 2g and h), which was the highest value demonstrated within all-carbon fiber-shaped solid DSSCs and even higher than the liquid cell reported elsewhere.[60] The aligned CNT core functioned as conducting scaffolds and supporting substrate, while the QDs (CdSe and CdS) dispersed in the CNT-based hybrid structure can realize both multiple exciton generation effects and multiple electron transmission paths to improve the energy conversion efficiency of DSSC. Moreover, the DSSC shows

Table 1 Performance comparison of reported fiber-shaped solar cell composed of different photoanodes and counter electrodes

Type	Counter electrode	Photoanode	V_{oc} (V)	J_{sc} (mA cm^{-2})	FF (%)	PCE (%)	Ref.
DSSC	CNT fiber	Bare CNT fiber	0.08	3.4	23	0.06	58
DSSC	CNT fiber	Random TiO_2/CNT	0.63	7.72	48	2.32	58
DSSC	CNT fiber	Aligned TiO_2/CNT	0.69	9.84	57	3.90	58
DSSC	CNT fiber	Mesoporous TiO_2/CNT	0.64	10.06	45	2.94	59
DSSC	CNT fiber	CNYs@TiO_2/CdS/CdSe	0.826	16.3	~53	7.39	60
DSSC	CNT/Pt fiber	Ti@TiO_2 fiber	0.54	15.3	59	4.85	61
DSSC	CNT/GNR/Pt fiber	Ti@TiO_2 fiber	0.69	13.55	72.6	6.83	63
DSSC	RGO/CNT/Pt fiber	Ti@TiO_2 fiber	0.73	17.6	—	8.50	64
DSSC	CNT fiber	Ti@TiO_2 fiber	0.72	9.7	55	4.6	65
DSSC	Pt/CS–CNT composite fiber	Ti@TiO_2 fiber	0.725	19.43	71	10	66
DSSC	CoSe/MWCNT fiber	Ti@TiO_2 fiber	0.72	13.78	65	6.70	67
DSSC	CNT/Pt fiber	Ti@TiO_2 fiber	0.73	16.99	64	8.10	68
DSSC	MWCNT arrays	Ti@TiO_2 fiber	0.71	16.00	61	7.10	69
Quasi-solid-state DSSC	CNT sheet	Ti@TiO_2 fiber	0.61	7.29	59	2.6	70
DSSC	CNT fiber	Ti@TiO_2 wire	0.68	15.69	66	7.01	71
Polymer solar cells	CNT fiber	Ti@TiO_2 wire	0.42	0.98	36	0.15	72
Polymer solar cells	MWCNT fiber	TiO_2 modified Ti wire	0.52	9.06	38	1.78	73
Polymer solar cells	CNT yarns	Steel@ZnO wire	0.55	8.1	~50	2.30	74
Perovskite solar cells	CNT sheet	Ti@TiO_2 fiber	0.86	14.5	56	7.10	78
Perovskite solar cells	CNT@Ag	CNT@TiO_2/$CH_3NH_3PbI_{3-x}Cl_x$	0.615	8.75	56.4	3.03	79
Perovskite solar cells	Elastic CNT fiber	Ti/TiO_2/$CH_3NH_3PbI_{3-x}Cl_x$	0.754	16	47	5.22	80

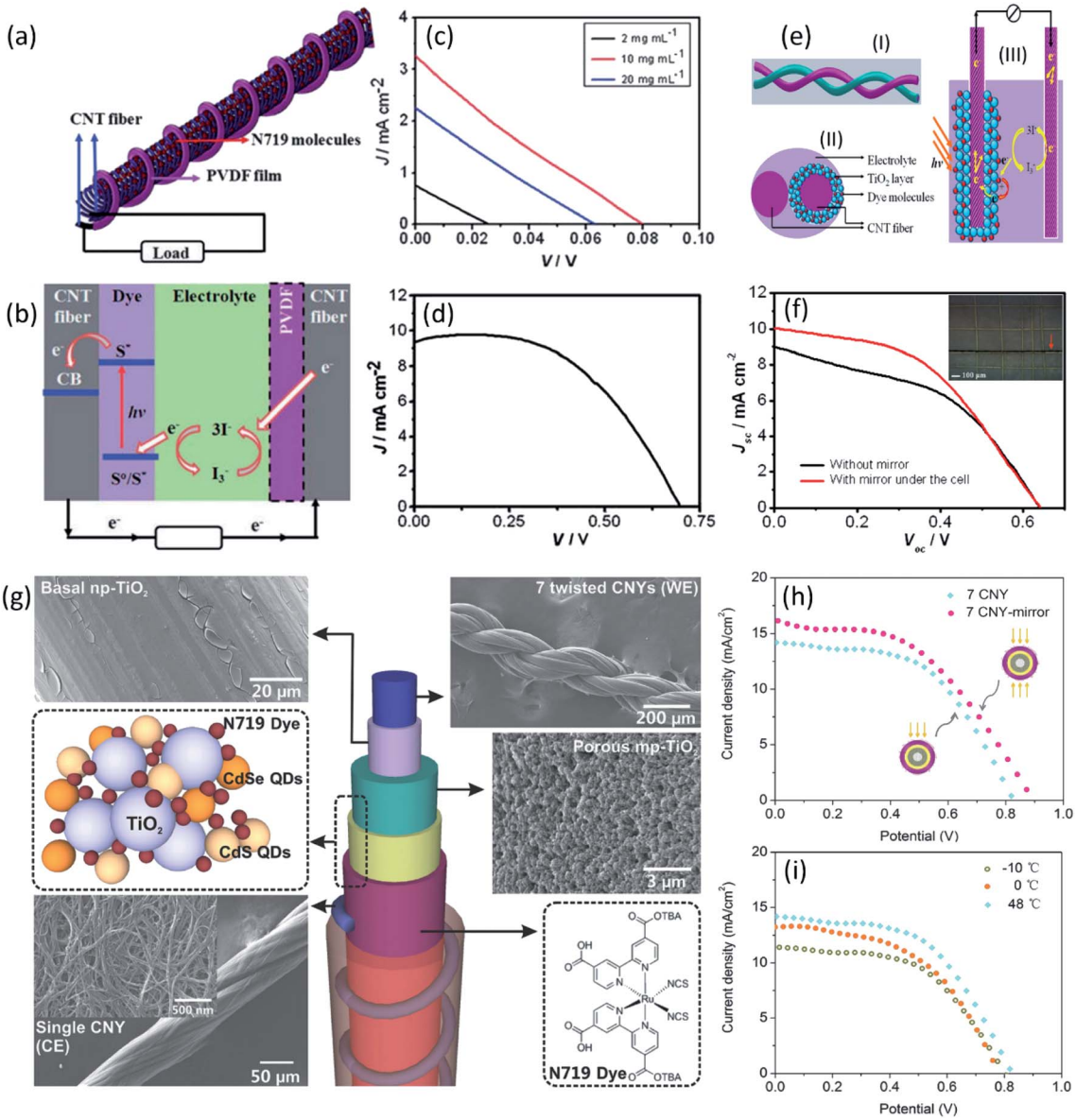

Fig. 2 (a) Schematic of a photovoltaic wire with two twined CNT fibers as working and counter electrodes, respectively. (b) The working principle of the photovoltaic wire. (c) *J*–*V* curves of photovoltaic wires by using CNT/PVDF fibers prepared with different PVDF concentrations as counter electrodes and CNT/N719 composite fiber as working electrode. (d) *J*–*V* curve using aligned titanium dioxide nanotubes on Ti wire as the working electrode.[58] Copyright 2012, Royal Society of Chemistry. (e) Schematic illustration and working mechanism of a wire-shaped DSSC fabricated from two CNT fibers. (f) *J*–*V* curves of a 1.1 cm long fiber cell without and with the use of a mirror, the inset illustrates a fiber cell being woven into a textile composed of aramid fibers.[59] Copyright 2012, American Chemical Society. (g) 3D wire-shaped DSSC using a platinized CNT fiber as counter electrode, a braid of 7-twisted CNT fibers with hybrid coatings as the working electrode. (h) *J*–*V* curves of wire-shaped hybrid cell with and without a mirror beneath. (i) *J*–*V* curves of wire-shaped hybrid cells with different temperature.[60] Copyright 2014, Wiley-VCH.

excellent thermal property with slight change of J_{sc} and V_{oc} at the working temperatures from −10 to 48 °C (Fig. 2i).

In addition to working electrode, the aligned CNT fibers can also serve as counter electrodes due to the high surface area and catalytic properties. However, compared with platinum, the pristine aligned CNT fiber has exhibited lower electrocatalytic activities due to less catalytic active sites such as defects and edge positions. To improve the catalytic performance towards efficient redox reaction of I_3^-/I^-, platinum nanoparticles and/or hydrophilic carbon materials (*i.e.*, graphene and hydrophilic CNTs) have been introduced into the aligned CNT fibers.[61–65] A PCE as high as 6.38% has been achieved by using core–sheath Pt-modified CNT/graphene nanoribbons as cathode (Fig. 3a and b), higher than the PCE of 5.31% in the case of CNT/Pt fiber cathode (Fig. 3c).[63] The highly aligned CNT fibers provided outstanding tensile strength and fast charge transport, and the graphene nanoribbons incorporated with Pt particles in the sheath expose more edges enabling a high electrocatalytic activity for I_3^-/I^- redox. The PCE was further increased to 8.50% by Hao *et al.* through utilizing novel graphene/CNT composite

fibers as the robust and conducting scaffolds for Pt in counter electrode (Fig. 3d and e).[64] Different from the core–sheath CNT/graphene structure, graphene incorporated among neighboring CNTs can serve as effective bridges to improve the charge transport because of strong π–π interactions between CNT and graphene sheet. Moreover, the graphene provides the efficient active sites to catalyze the redox reaction of I_3^-/I^- as well as surface area for the deposition of Pt nanoparticles to further improve both high electrical conductivity and electrocatalytic activity of the DSSCs. In addition to graphene, hydrophilic CNTs with more active sites showed higher electrochemical activities than hydrophobic CNTs. Through the surface modification of CNTs, a record PCE of 10% was achieved by using Pt-electrodeposited hydrophobic core/hydrophilic sheath CNT fibers as counter electrodes (Fig. 3f).[66] The hydrophilic sheath containing functional groups and active defects provided more nucleation sites for small Pt nanoparticle deposition, greatly improving the catalytic activity. Despite a significant improvement in the electrocatalytic activity, high-cost Pt compulsion in the cathodes still remained the major drawback. Besides Pt, some inorganic compounds (*i.e.*, carbides and sulfides *etc.*), especially selenium-based nanoparticles currently as the second phase are also introduced in the CNT fibers due to its high electrocatalytic activity and low-cost. Ali *et al.* reported a fiber-shaped DSSC using CoSe-modified CNT fiber as the counter electrode, as shown in Fig. 3g and h.[67] The CoSe on MWCNTs fibers effectively enhances the surface area and prove an ideal phase to catalyze the electrons transfer even more effectively. Coupled with TiO_2/N719 modified Ti wire as working electrode, the obtained fiber-shaped DSSC showed a much higher PCE of 6.7% than the device using pristine MWCNTs fibers with PCE of 3.97% (Fig. 3i).

As discussed above, great achievements on the CNT fiber-based fiber-shaped DSSCs have been made with a variety of designs.[68,69] Accompanied with the continuously increasing PCE, the mechanical stability and compatibility of the fiber-shaped DSSCs also showed significant improvement by

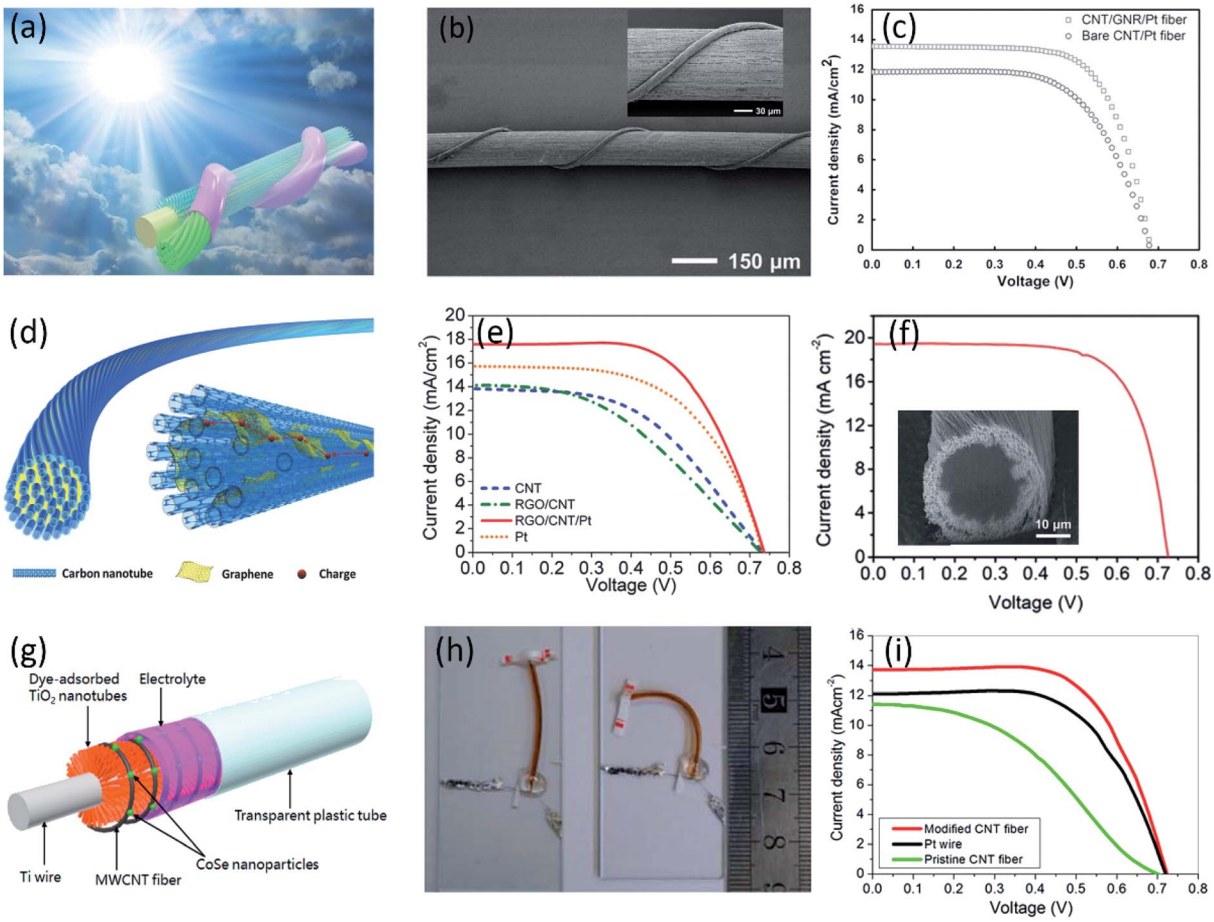

Fig. 3 (a) Schematic of wire-shaped DSSC with core–sheath nanostructured fiber as a cathode. (b) SEM images of a wire-shaped DSSC at low and high magnifications (the inset). (c) *J*–*V* curves of wire-shaped DSSCs with bare CNT and CNT/GNR fibers both deposited with Pt nanoparticles as cathodes.[63] Copyright 2014, Wiley-VCH. (d) Schematic illustration to the structure of the graphene/CNT composite fiber. (e) *J*–*V* curves of wire-shaped DSSCs with bare CNT, graphene/CNT, graphene/CNT/Pt and bare Pt fibers as the cathodes.[64] Copyright 2014, Wiley-VCH. (f) *J*–*V* curve of the fiber-shaped DSSC with the highest PCE. The inset shows cross-sectional SEM image of the core–sheath fiber containing 25% modified CNTs as the sheath.[66] Copyright 2018, Royal Society of Chemistry. (g) Schematic of the Pt-free flexible fiber-shaped DSSC. (h) Optical image of the bend device. (i) *J*–*V* curves of fiber-shaped devices with different counter electrodes.[67] Copyright 2016, American Chemical Society.

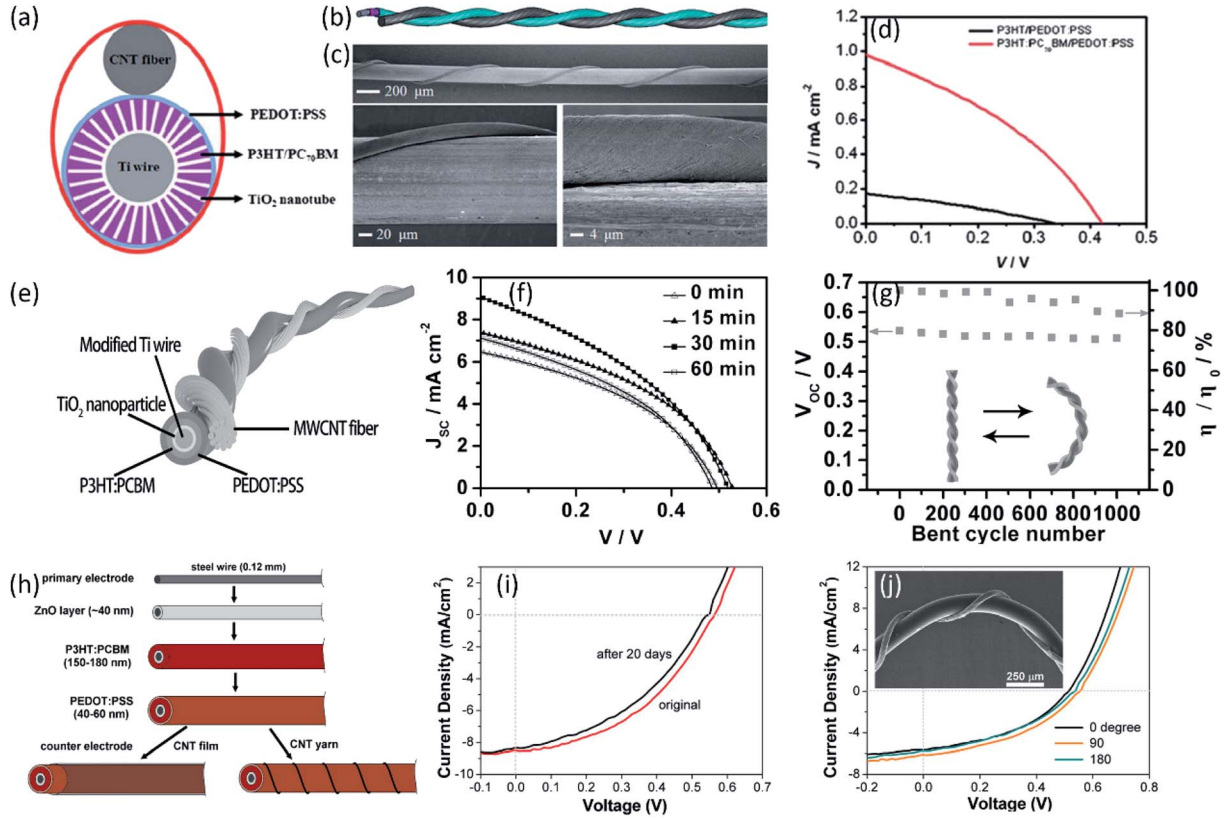

Fig. 4 (a) and (b) Schematic illustration of a polymer photovoltaic wire from top and side views, respectively. (c) SEM images of a middle part of a PSC wire at the low and high magnification. (d) *J*–*V* curves of typical PSC wires with and without $PC_{70}BM$.[72] Copyright 2012, Royal Society of Chemistry. (e) Schematic illustration to the wire-shaped PSC. (f) *J*–*V* curves without and with $TiCl_4$ treatments under the increasing growth time. (g) Dependence of PCE and voltage on bent cycle number.[73] Copyright 2014, Wiley-VCH. (h) Illustration of the fiber-shaped solar cell (FSC) structure and fabrication process. (i) *J*–*V* curves of a FSC in original state and after storage in inertia gas for 20 days. (j) *J*–*V* curves of a FSC in straight form (0 degree) and bent to 90 and 180 degrees, respectively. Inset shows the SEM image of the FSC twisted by a CNT yarn electrode and bent to 90 degrees.[74] Copyright 2012, American Chemical Society.

replacing traditional metal wire with aligned CNT fiber. Nevertheless, existing problems such as the leakage, toxicity, and vaporization of electrolyte, make it impossible to integrate the flexible fiber-shaped DSSCs into wearable device. Although a PCE as high as 7.39% has been achieved in a novel design of core–sheath solid state DSSC using CNT yarns with hybrid structure, much more breakthroughs are urgently needed.[70,71]

Compared with fiber-shaped DSSCs based on the dye molecules, fiber-shaped polymer solar cells (PSCs) are more suitable for wearable devices due to their all-solid-state structure. Presently an interpenetrating structure between polymeric donor and fullerene acceptor was generally designed to enhance the charge separation and transport due to a high interfacial area in polymer photovoltaics. Chen *et al.* reported fiber-shaped PSCs with an aligned CNT fiber as the cathode.[72] Twined with a Ti/TiO_2 wire anode, the photovoltaic wires achieved the PCE of 0.15%, where the poly(3-hexyl-2,5-thiophene) (P3HT) and (6,6)-phenyl-C71 butyric acid methyl ester ($PC_{70}BM$) were used as photoactive materials, as shown in Fig. 4a–d. After optimizing the TiO_2 structure, a much higher efficiency of 1.78% was realized in the CNT fiber-based PSCs (Fig. 4e and f).[73] Ascribed to the outstanding flexibility and structure stability of the aligned CNT fibers, the obtained fiber-shaped devices could be woven into various flexible structures such as textiles without further sealing. The PCE of the textiles could maintain 85% of the initial value after bending for 1000 cycles, as shown in Fig. 4g. Liu *et al.* developed a novel organic photovoltaic fiber by using aligned CNT fiber as cathode and ZnO-modified steel wire as photoanode (Fig. 4h–j), achieving the enhanced PCE of 2.3%.[74]

Although much efforts have been devoted to improve the charge transport and optimize optical absorption, the current low PCE of fiber-shaped PSCs still can't satisfy the practical applications, which should be further improved. In addition to the polymer solar cells, fiber-shaped perovskite solar cells have attracted worldwide attention due to liquid-free electrolyte, in which perovskite layer is sandwiched between electron and hole transport materials. Although the current power conversion efficiency of 10.79% has been already achieved, the used noble metal of Au fiber and film greatly increase the cost and weight of the fiber-shaped perovskite solar cells, limiting its practical application.[75] Compared with noble metal, CNT fiber has been considered as the potential candidate electrodes for high performance fiber-shaped perovskite solar cells due to its

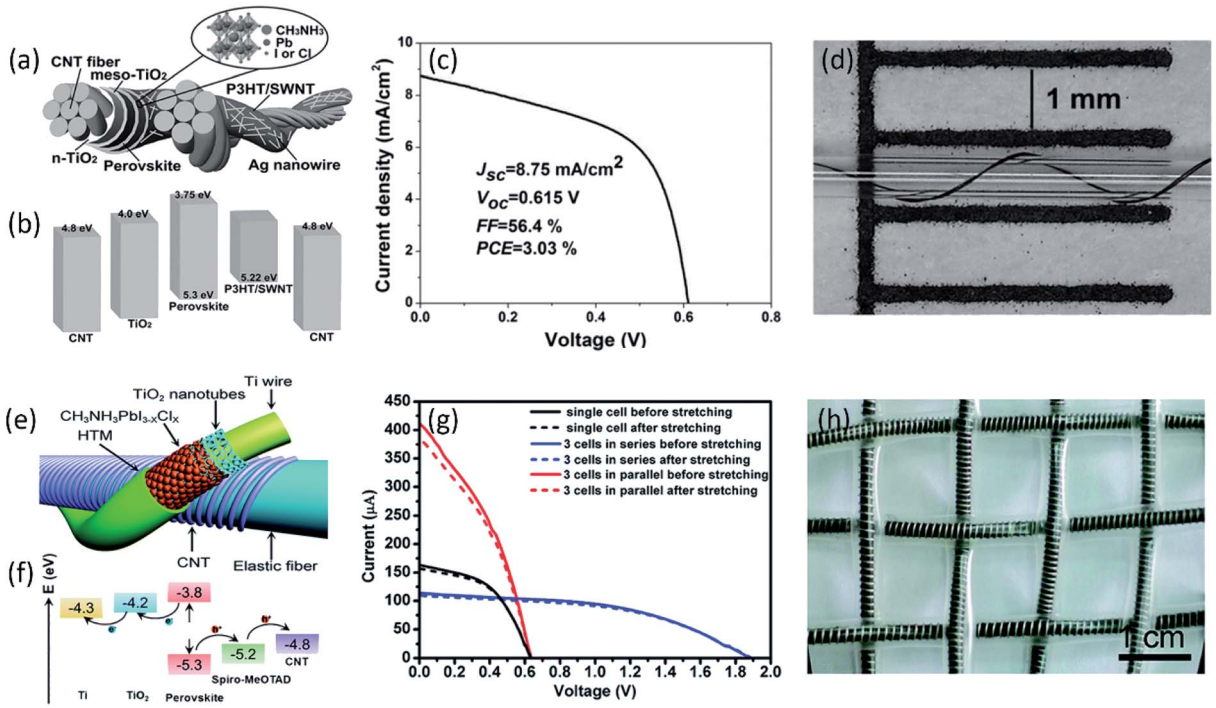

Fig. 5 (a) Structure and (b) energy-level diagram (relative to the vacuum level) of each layer in the double-twisted fibrous perovskite solar cell. (c) *J*–*V* curve of the double-twisted fibrous perovskite solar cell with the best PCE of 3.03%. (d) The photograph of the double-twisted fibrous perovskite solar cell wrapped onto a capillary tube with curvature radius of 0.3 mm.[79] Copyright 2015, Wiley-VCH. (e) Schematic illustration to the elastic perovskite solar cell fiber structure and (f) energy level diagram. (g) *J*–*V* curves of the resulting powering textile where three perovskite solar cell fibers were connected in series or parallel before and after stretching. (h) Photograph of an elastic powering perovskite solar cell textile.[80] Copyright 2015, Royal Society of Chemistry.

outstanding flexibility, lightweight, and high catalytic activity.[76–78] Li *et al.* reported a CNT fiber-supported double-twisted perovskite solar cell with PCE of 3.03%, as shown in Fig. 5a–d, which was higher than the fiber-shaped polymer solar cell.[79] A thin layer of $CH_3NH_3PbI_{3-x}Cl_x$ coated on the highly flexible CNT fiber here possesses a higher charge carrier mobility and simultaneously shows excellent structural stability under bending for more than 1000 cycles without degradation. The higher PCE of 5.22% has been achieved by designing a stretchable fiber-shaped perovskite solar cell with CNT fiber and spring-like Ti wire as two electrodes (Fig. 5e–g). The aligned CNT sheet was closely attached to the conductive elastic fiber to increase the hole collection, effectively increasing the energy conversion efficiency. Moreover, ascribed to the highly elastic fiber and flexible CNT fiber, the fabricated devices exhibited stable photovoltaic performance under both stretching and bending when they were woven into electronic textiles (Fig. 5h).[80] Despite the great achievement, the efficiency of CNT fiber-based perovskite solar cells was still much lower than the traditional planar perovskite solar cell (PCE > 20%), limiting the practical application. This result was mainly ascribed to poor interface contact and charge transfer between photoactive layer and CNT electrodes. Through the optimized modification and functionalization of aligned CNT fiber electrode, the fiber-shaped perovskite solar cell possesses the great potential to achieve the PCE equal to or even higher than the fiber-shaped DSSCs.

3.2 Fiber-shaped supercapacitors

Aligned CNT fibers with excellent conductivity, outstanding mechanical properties and high specific surface area are promising for constructing fiber-shaped supercapacitors.[81–85] However, the lower energy density of CNT fiber-based fiber-shaped supercapacitor resulted in frequent charge/discharge during practical application, difficult to satisfy the actual requirement. According to the equation $E = CV^2/2$, the energy density (E) is proportional to specific capacitance (C). Recently, much efforts have been made to increase the specific capacitance through introducing high pseudocapacitive materials such as carbonaceous active materials (*i.e.*, porous carbon, graphene oxide),[86] conducting polymers (*i.e.*, PANI, PPy and PEDOT) and transition metal oxides (*i.e.*, MnO_2, Fe_2O_3 and Co_3O_4) into the aligned CNT fibers.[82,87–96] Wang *et al.* reported a synchronous deposition strategy to continuously fabricate fiber-shaped supercapacitors based on aligned CNT/RGO composite fibers, as shown in Fig. 6a.[86] The oxygen-containing moieties (like carbonyl group and carboxyl group) on the basal plane of RGO provide rich active sites for pseudocapacitance which is dominantly contributed to the enhancement of capacitance. As a result, the obtained twisted fiber-shaped supercapacitor possessed a high specific capacitance of 68.4 F cm^{-3} at 31 mA cm^{-3} and an energy density of 2.4 mW h cm^{-3}, higher than the bare CNT fiber-based supercapacitor (4.5 F cm^{-3} at 31 mA cm^{-3}) (Fig. 6b and c). Moreover, benefiting from

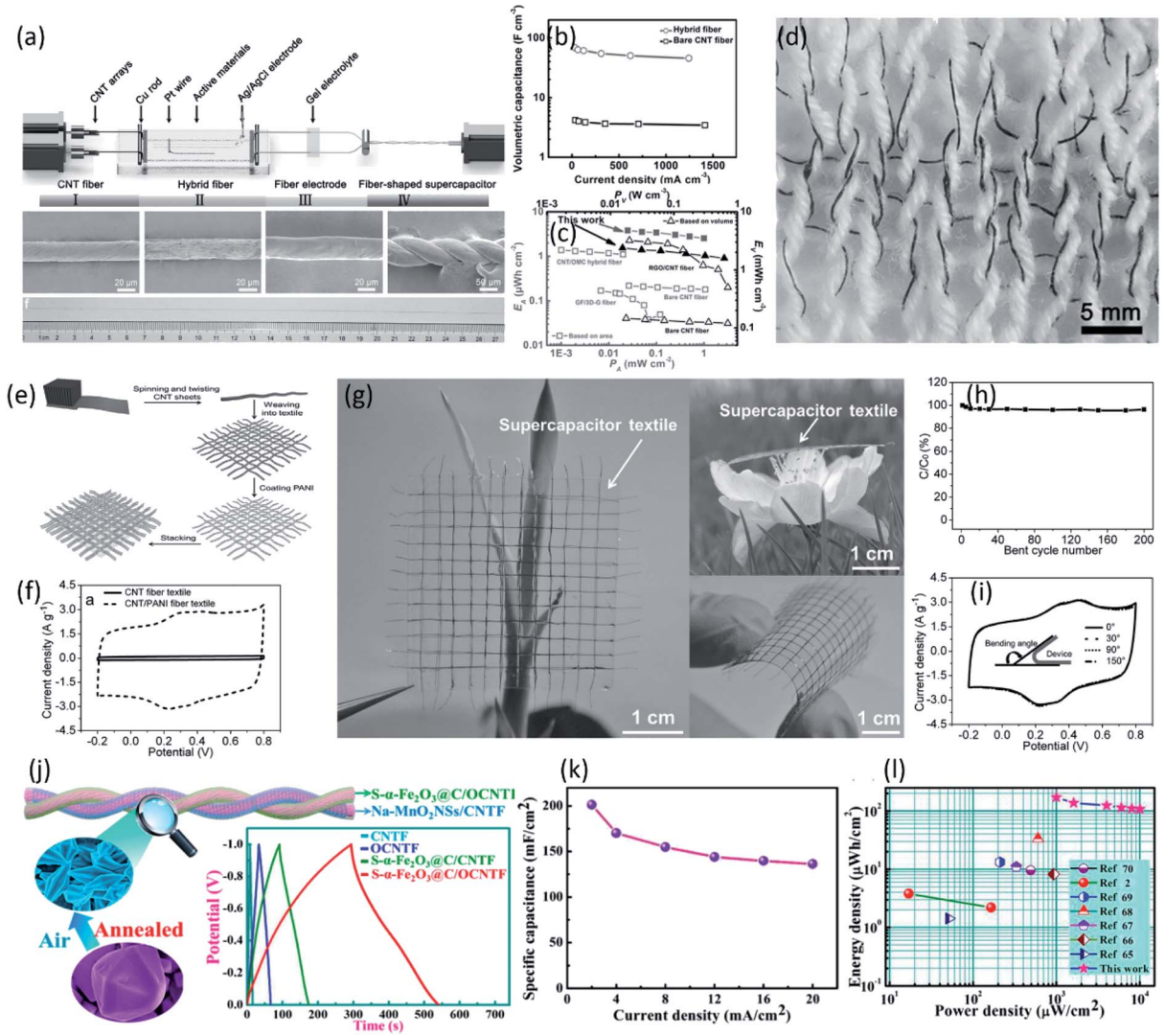

Fig. 6 (a) Schematic of the experimental setup for the continuous fabrication of supercapacitor fiber and the SEM images of fiber electrode and supercapacitor fiber. (b) Volumetric capacitances of supercapacitor fiber at increasing current densities. (c) Ragon plot of the supercapacitor fiber based on different carbonaceous fibrous electrodes. (d) An integrated fabric woven from cotton yarns (white fibers) and supercapacitor fibers (black fibers).[86] Copyright 2015, Wiley-VCH. (e) Schematic illustration to fabrication of a supercapacitor textile based on the CNT/PANI composite fiber. (f) CV curves of bare CNT fiber-based textile and CNT/PANI composite fiber-based textile. (g) Photographs of a transparent supercapacitor textile. (h) Dependence of specific capacitance on bend cycle number of a supercapacitor textile (bending angle of 150°). (i) CV curves of a supercapacitor textile being bent into different angles at a scan rate of 20 mV s^{-1}.[87] Copyright 2015, Wiley-VCH. (j) Schematic illustration of the fiber-shaped asymmetric supercapacitor. The inset shows the comparison of galvanostatic charge–discharge curves of different electrodes at a current density of 5 A g^{-1} (4 mA cm^{-2}). (k) Areal specific capacitances of the fiber-shaped supercapacitors as a function of the current density. (l) Areal energy and power densities of the device in comparison with previously reported values.[91] Copyright 2018, American Chemical Society.

the high strength and flexibility of CNT composite fiber, the fiber-shaped supercapacitors could be knitted into textile without structure damage, suggesting potential application in wearable electronics (Fig. 6d). In addition to carbonaceous materials, conducting polymers have been also widely used in supercapacitors due to their high specific capacitance and flexibility.[86,97] Pan *et al.* prepared a novel wearable energy device based on aligned CNT/PANI fiber textiles, as shown in Fig. 6e and f.[87] Due to the remarkable electrochemical activity of PANI and outstanding flexibility of aligned CNT fiber, the resulting supercapacitor textile showed a higher specific capacitance of ~196.3 F cm^{-3} which could maintain 96.4% after bending for 200 cycles (Fig. 6g–i).

Compared with conducting polymers, transition metal oxides are regarded as the promising candidates for supercapacitor electrode materials due to its high theoretical specific capacitance, low cost and easy availabilities. However, the poor intrinsic conductivity and severe aggregation of transition metal oxides severely hinders the charge transfer during redox reaction, resulting in compromises of power density and cycling stability as well as lower specific capacitance than theoretical value. Combining the aligned high-conductive CNT fiber with

transition metal compounds for pseudo-capacitance is an effective way to increase the intrinsic capacitance of fiber-shaped supercapacitors. Lu *et al.* reported the utilization of CNT/MnO_2 composite fiber electrodes for micro-supercapacitor wire.[88] The CNT fiber on the one hand act as conductive collector ensuring fast charge transport, on the other hand provide sufficient surface area for deposition of MnO_2. The MnO_2 nanoflakes orderly deposited on the surface of aligned CNT fiber without serious aggregation expose more surface area for pseudo-capacitance. As a result, the assembled fiber-shaped symmetric supercapacitor demonstrated a high specific capacitance of 156 F cm^{-3} in LiCl/PVA electrolyte. Similar with MnO_2, other metal oxides, such as Co_3O_4, NiO, Fe_2O_3 *etc.*,[83] have also been commonly used for supercapacitors due to their high theatrical specific capacitance, environmental compatibilities, and low cost. Zhou *et al.* designed a porous S-α-Fe_2O_3@C on the oxidized aligned CNT fiber as anode for high-performance wearable asymmetric supercapacitors, as shown in Fig. 6j.[91] Due to the ultrahigh surface area and excellent conductivity, the S-α-Fe_2O_3@C/OCNTF electrode exhibited a superior areal capacitance of 1232.4 mF cm^{-2} at 2 mA cm^{-2} and an excellent rate capability (Fig. 6j). Twisted with Na-doped MnO_2 nanosheets/CNT composite fiber, the asymmetric fiber-shaped supercapacitors exhibited a high specific capacitance of 201.3 mF cm^{-2} and an exceptional energy density of 135.3 μW h cm^{-2} (Fig. 6k and l). Sun *et al.* developed the hierarchically-structured Co_3O_4 nanowire arrays grown on CNT fibers to serve as novel cathodes for high-performance wearable fiber-shaped asymmetric supercapacitors.[90] The well-aligned three-dimensional cobalt oxide nanowire arrays (Co_3O_4 NWAs) directly deposited on carbon nanotube fibers (CNTFs) not only enlarge electrode–electrolyte contacting area for electrochemical reaction (Co_3O_4 ↔ CoOOH), but also provide a short diffusion path for fast ion transport. The obtained hybrid fibers showed an ultrahigh specific capacitance of 734.25 F cm^{-3} (2210 mF cm^{-2}) in a three-electrode system. Coupled with the vanadium nitride nanowires/CNT fibers, the fabricated asymmetric fiber-shaped supercapacitors possessed a high energy density of 13.2 mW h cm^{-3} in KOH/PVA gel electrolyte with a stable potential window of 1.6 V. To further increase the electrochemical performance of the aligned CNT fiber electrode, polynary metal oxides/CNT hybrid electrodes have been developed,[98] such as Zn–Ni–Co ternary oxides (ZNCO),[99,100] Mo–Ni–Co ternary oxide (MNCO),[89] due to their higher electrochemical activity and conductivity than the ones using mono-metal oxide and binary-metal oxide. Sun *et al.* prepared a wearable fiber-shaped asymmetric supercapacitor with a maximum operating voltage of 1.6 V by utilizing hierarchical dandelion-like MNCO/CNT fiber as the positive electrode.[89] The optimized device exhibited a remarkable specific capacitance of 62.3 F cm^{-3} (233.7 mF cm^{-2}), a high energy density of 22.2 mW h cm^{-3} (83.1 μW h cm^{-2}) and an extraordinary power density of 2133.3 mW cm^{-3} (8000 mW cm^{-2}).

In addition to transition metal oxide, transition metal sulfide and transition metal nitride have also attracted great interests.[101–103] Zong *et al.* developed a twisted asymmetric supercapacitor composed of MoS_2/CNT composite fiber as negative electrode and Na-doped MnO_2/CNT composite fiber as positive electrode.[101] Benefiting from the excellent electrochemical activity of transition metal compounds and high conductivity of aligned CNT fiber, the fabricated asymmetric supercapacitor showed an incredible specific capacitance of 265.4 mF cm^{-2}, an ultrahigh energy density of 178.4 μW h cm^{-2}, and outstanding flexibility (120° bending, over 3500 times) with the high operating voltage of 2.2 V. Among the transition metal nitrides, vanadium nitride (VN) has been considered as a promising anode material for asymmetric supercapacitors due to its large specific capacitance (1340 F g^{-1}) and superb electrical conductivity (10^6 Ω m^{-1}).[89,90,96,99,100,102] Especially, the aligned porous VN can provide higher specific surface area for faradic reaction and more ion transport path. Based on the VN@C nanowire arrays/CNT fibers as core electrode, the asymmetric coaxial fiber-shaped supercapacitors were developed with a high specific capacitance of 213.5 mF cm^{-2} and an exceptional energy density of 96.07 μW h cm^{-2}.[102]

Moreover, stretchable/elastic CNT-based yarn supercapacitors currently are particularly attractive for wearable electronics in practical applications, especially inevitable severe defamation in daily life.[104] Choi *et al.* report a bi-scrolled yarn MnO_2/CNT fiber electrode. The CNT here provide strength and electrical conductivity. Despite the high loading of MnO_2, the final bi-scrolled solid-state yarn supercapacitors can be made elastically stretchable (up to 30% strain) by over-twisting to produce yarn coiling.[105] Similarly, the buckled CNT fiber electrode was also prepared for highly stretchable/elastic yarn supercapacitors, which can effectively absorb tensile or shear stresses during the severe deformation and can sustain up to 1500% elastic deformation. Consequently, by incorporating pseudocapacitive-active materials, the fabricated super-elastic fiber-shaped supercapacitors show high linear and areal capacitance values of 21.7 mF cm^{-1} and 92.1 mF cm^{-2}, respectively, that can be reversibly stretched by 1000% without significant capacitance loss, showing great wearable applications.[106]

3.3 Fiber-shaped lithium-ion batteries

Fiber-shaped lithium-ion batteries (LIB) are the promising energy devices to power the portable and wearable electronics due to their high energy density. Their electrochemical and mechanical performances are highly dependent on the design of composite fiber electrodes. Among various fiber electrodes, CNT-based composite fiber has been considered as one of the most potential candidate electrodes for highly stable and flexible fiber-shaped batteries.[19,107–110] Usually, bare CNT fiber can provide strong mechanical scaffold, fast charge transport pathway and high specific surface area for loading active materials (*i.e.*, MnO_2, MoS_2, Si, $Li_4Ti_5O_{12}$ (LTO) and $LiMn_2O_4$ (LMO), *etc.*) to improve enhance the performance of LIB.[83,92,111–118] Ren *et al.* fabricated a novel CNT fiber-based fiber-shaped LIB through twisting MnO_2 modified CNT fiber (positive electrode) together with Li wire (negative electrode) (Fig. 7a).[92] Ascribed to the higher Li^+ intercalation/deintercalation potential of aligned MnO_2/CNT fiber compared with bare CNT fiber,

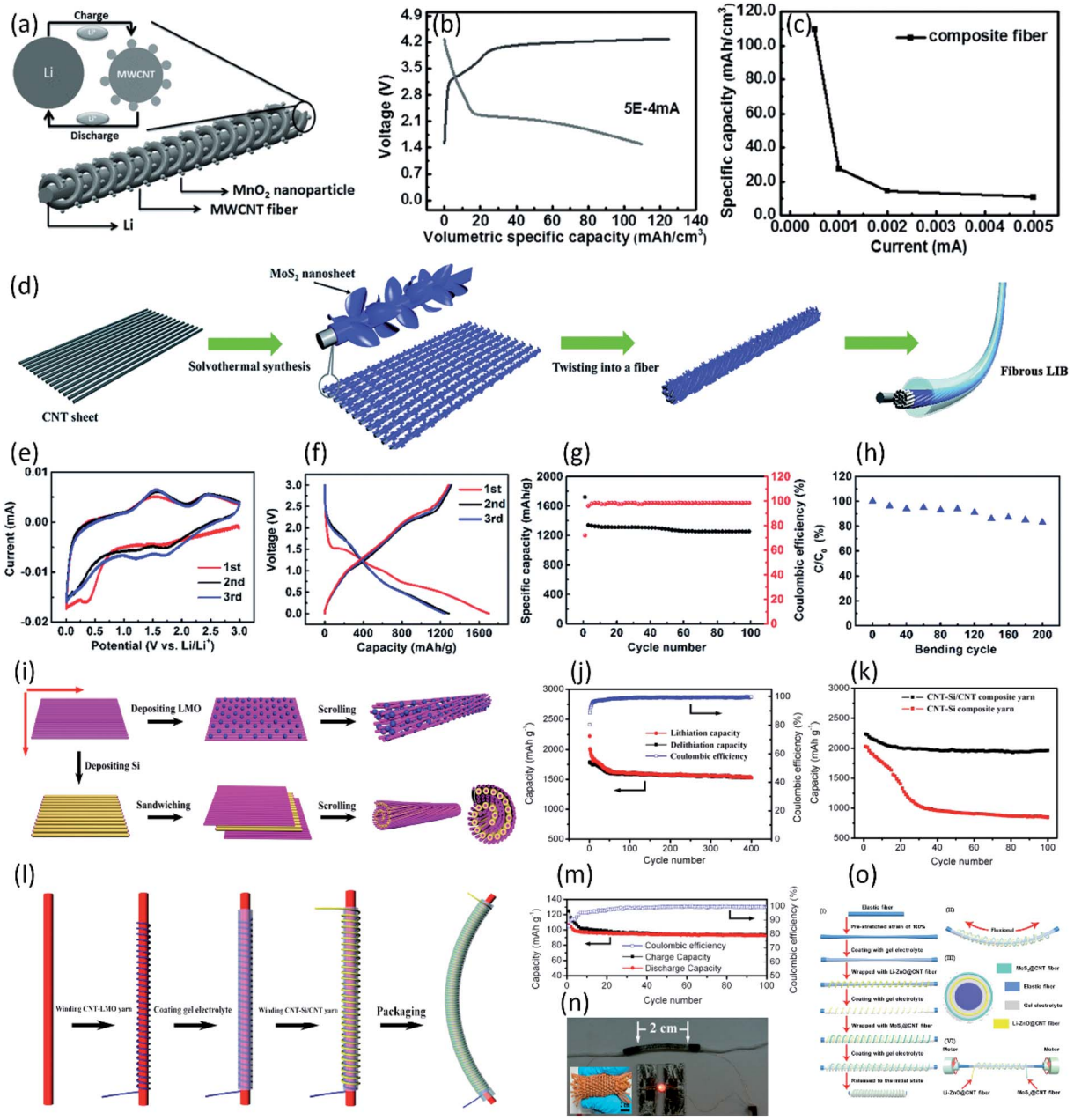

Fig. 7 (a) Schematic illustration to the wire-shaped LIB fabricated by twisting an aligned MWCNT/MnO_2 composite fiber and Li wire as positive and negative electrodes, respectively. The inset top left image shows the charge–discharge process. (b) Charge and discharge of wire-shaped LIB with a MWCNT/MnO_2 composite fiber and Li as electrodes. (c) Dependence of specific capacitance for a battery wire on current.[92] Copyright 2013, Wiley-VCH. (d) Schematic illustration of the synthesis of the aligned CNT/MoS_2 hybrid fiber and the structure of the fibrous LIB. (e) Cyclic voltammograms of the fibrous LIB with the aligned CNT/MoS_2 hybrid fiber as the cathode at 0.1 mV s^{-1}. (f) The first three charge–discharge curves of the fibrous LIB at 0.2 A g^{-1}. (g) Cycling performances of the fibrous LIB at 0.2 A g^{-1}. (h) Dependence of specific capacity on the bending cycle.[112] Copyright 2015, Royal Society of Chemistry. (i) Schematic illustration of the synthesis of high-performance composite yarns. (j) Long-life performance of the CNT–Si/CNT composite yarn at 2C. (k) Comparison of cyclic performances between CNT–Si and CNT–Si/CNT composite yarns at 0.4C. (l) Schematic illustration to the fabrication of the coaxial fiber full LIB. (m) Long-life performance of the fiber-shaped LIB between 2.0 and 4.3 V at 1C. (n) Photograph of a fiber-shaped LIB to lighten up a LED and fiber-shaped full LIBs being woven into a textile (inset).[113] Copyright 2014 American Chemical Society. (o) Schematically showing the (I) fabrication process, (II) stretchability representation, (III) cross-sectional view of the stretchable fiber-like Li metal battery, and (VI) wrapping of the Li–ZnO@CNT fibers around a pre-stretched elastic fiber.[118] Copyright 2019, Elsevier.

a specific capacity of 109.62 mA h cm^{-3} (or 218.32 mA h g^{-1}) for the battery in 1 M $LiPF_6$ electrolyte solution had been achieved (Fig. 7b and c). In addition to the MnO_2 nanoparticles, the MoS_2 is widely appreciated as an alternative material for LIBs due to its high energy storage capacity. Luo *et al.* reported a novel aligned MoS_2 nanosheet/CNT hybrid fiber to serve as positive

electrode for fiber-shaped LIB (Fig. 7d).[112] The MoS_2 nanosheets directly wound on the surface of the CNT provide large specific surface area for energy storage. The designed hybrid nanostructure efficiently combined the superiority of high electrical conductivity in the CNT and high energy storage capacity in MoS_2. Paired with a lithium wire anode, the obtained fiber-shaped LIB showed a high specific capacity of 1298 mA h g^{-1} and excellent cycle stability with the capacity retention of 1250 mA h g^{-1} after 100 cycles at 0.2 A g^{-1} (Fig. 7e–h). To further improve the specific capacity, the Si modified CNT fiber has been studied as a promising electrode material, due to the ultrahigh theoretical capacity (4200 mA h g^{-1}) of Si and high conductivity of aligned CNT fiber. Lin *et al.* developed novel twisted and aligned Si/multiwalled CNT (MWCNT) composite fiber electrodes for fiber-shaped LIB using a Li wire as the counter electrode.[115] When the weight percentage of Si in the Si/CNT composite fiber was controlled around 38.1%, the fiber-shaped LIB achieved the high specific capacity of 1670 mA h g^{-1} at current density of 1.0 A g^{-1}. Higher specific capacity of 2200 mA h g^{-1} has been achieved by Sun *et al.*, using Si-coated CNT yarn as electrode due to its outstanding flexibility and electrical conductivity.[116] Although high performance can be achieved by introducing Si particles into the CNT fiber, the huge volume change of Si during the lithiation/delithiation process results in a fast capacity decay. To solve this problem, a novel CNT–Si/CNT composite yarn was synthesized by Weng *et al.* (Fig. 7i).[113] Here, the special hybrid layered structure was conducive to buffering the volume change of Si and clamping the Si layer, ensuring the structure stability of electrode during lithiation/delithiation process. To investigate the electrochemical property of the composite yarns, the half-cell fiber-shaped LIB was fabricated with a lithium wire as the counter electrode. For the CNT–Si/CNT composite yarn, a specific capacity of 2240 mA h g^{-1} could be obtained at the first cycle with 88% retention after 100 cycles, exhibiting higher cycle stability than Si/CNT composite yarn under the same condition (42% capacity retention, Fig. 7j and k). Based on the researches above, half-cell fiber-shaped LIB showed outstanding specific capacity. However, metal Li wire anode limit the flexibility of fiber-shaped LIB. Moreover, the liquid electrolyte used in above fiber-shaped LIBs hampered practical applications due to the problems of leakage and complex packaging. By replacing the metal Li wire with CNT–$LiMn_2O_4$ (LMO) yarn, the coaxial fiber-shaped full LIB with gel electrolyte was finally fabricated with the CNT–Si/CNT and CNT–LMO composite yarns as the anode and cathode, respectively (Fig. 7l).[113] A specific discharge capacity of 106.5 mA h g^{-1} was achieved at the first cycle with the capacity retention of 87% after 100 cycles, as shown in Fig. 7m. Benefiting from the high flexibility of CNT-based composite fiber, the obtained full-cell fiber-shaped LIB could be further woven into a flexible textile (Fig. 7n).

In addition to electrolyte leakage of full-cell fiber-shaped LIBs, the safety issue arising from the growth of dendritic lithium on the anode surface (*i.e.*, Si anode) has also attracted great interests. To avoid this problem, much attention has been paid to developing the novel electrode materials with higher lithiation potentials and small volume change, such as spinel $Li_4Ti_5O_{12}$ (LTO), polyimide (PI) and ZnO.[111,114,117,118] Ren *et al.* introduced the LTO and LMO nanoparticles into the aligned CNT yarns. The obtained MWCNT/LTO and MWCNT/LMO composite yarns were used as anode and cathode, respectively, and were assembled into a full-cell fiber-shaped LIB with a belt separator and liquid electrolyte.[114] The full-cell achieved a high specific capacity of 138 mA h g^{-1} at 0.01 mA and a discharge volumetric energy density of 17.7 mW h cm^{-3}. Ascribed to the high flexibility of CNT-based composite fiber, the fiber-shaped LIB could be woven into various electronic textiles for wearable electronics. Moreover, an elastic wire-shaped LIB could also be fabricated by winding the MWCNT/LTO anode and MWCNT/LMO cathode yarns around an elastic substrate. The stretchable fiber-shaped battery showed the initial discharge capacity of 138 mA h g^{-1} with the retention of over 90% when the battery was stretched by 100%, exhibiting outstanding adaptability. Recently, a novel highly-stretchable fiber-shaped LIB with high capacity (1176 mA h g^{-1} at 50 mA g^{-1}) was developed using a Li–ZnO@CNT hybrid fiber as the anode, as shown in Fig. 7o.[118] Interestingly, the Li anode integrated the three-dimensional structure of ZnO arrays and the admirable stretchability of CNT fibers. When matched with MoS_2@CNT fibers, the stretchable fiber-like Li metal battery exhibited an excellent cyclic stability under a strain of 100% and a dendrite-free morphology after repeated plating/stripping cycling.

4. Conclusions and perspectives

This review mainly touched on the synthesis, physical properties, and applications of the aligned CNT fiber in energy harvesting and storage devices. The aligned CNT fibers with different physical properties (electrical and mechanical properties) can be prepared by spinning from CNT solution, CNT aerogel, aligned CNT array or twisting from CNT films. Ascribed to its lightweight, extraordinary mechanical strength, desirable conductivity and high specific surface area, the aligned CNT fibers have been widely considered as promising electrodes or conductive substrates in fiber-shaped solar cells, supercapacitors, and lithium-ion batteries. To improve the performance of fiber-shaped devices, many works have focused on designing novel aligned CNT-based composite fibers by introducing the second phases, such as carbonaceous materials, metal particles, conducting polymers and transition metal compounds, *etc.* Despite recent rapid advances, there is still a need to further improve material properties and enhance device performance.

For fiber-shaped energy harvesting devices, particularly fiber-shaped DSSCs, the aligned CNT fiber electrode which was used as working electrode (anode) should possess excellent electronic properties for fast charge transport and high specific surface area for efficient adsorption of dye molecules. Introducing a porous TiO_2 nanocrystal hole blocking layer on the aligned CNT fiber can effectively improve the photoinduced charge separation and transport of carriers to the electrode, leading to increased PCE. Meanwhile, the counter electrode (cathode) based on the aligned CNT composite fiber should possess outstanding catalytic properties. High conversion efficiencies can be achieved by replacing the conventional Pt wire with Pt modified CNT fiber as

counter electrode. Moreover, surface modification such as heteroatom doping can also improve the catalytic activity of CNT fiber-based electrode. While for the CNT fiber-based fiber-shaped polymer and perovskite solar cells, the PCE was presently lower than that of fiber-shaped DSSCs, which was mainly ascribed to poor interface contact between solid photoactive layer and CNT-fiber electrodes.

In addition, for flexible fibrous electrochemical energy storage devices, the aligned CNT fibers are promising candidates for electrode materials owing to their outstanding conductivity and high specific capacitances. However, a major challenge for CNT fiber electrodes is the low energy density. An effective strategy for solving this problem is introducing pseudocapacitive materials (such as conducting polymer, metal oxide, metal sulfide, *etc.*) into the aligned CNT fiber, which can greatly enhance the energy density of the devices. The porous pseudocapacitive materials on aligned CNT fiber are conducive to the fast ion transport and adapting the volume change during charge/discharge processes, ensuring rate capability and cyclic stability of the devices.

Overall, the aligned CNT fiber and its composite fiber are valuable electrode materials with great potential for fiber-shaped energy harvesting and storage devices. However, the relatively low performance of CNT fiber-based devices, especially all-solid energy devices, remarkably limits the practical applications. Therefore, more efforts should be made to design novel aligned CNT composite fiber electrodes with outstanding photoelectric or electrochemical activity through surface modification and functionalization for much higher performances. Another challenge is improvement of the structure stability (*i.e.*, strength and deformability) for fiber-shaped energy devices to effectively weave such fiber-shaped devices into textiles for stretchable, portable, wearable, deformable, and even implantable electronics. Usually, introducing the second phase or surface modification may decrease the electronic and mechanical properties of the aligned CNT fiber electrodes. To balance the electrochemical activity, conductivity, and mechanical properties of the aligned CNT composite fiber, regulating the interfacial properties and structure of active materials is critical. In summary, these CNT fiber-based energy devices are highly promising to achieve mass production and can be applied to wearable electronic devices such as consumer electronics, artificial electronic skins in our future life.

Conflicts of interest

There are no conflicts to declare.

Acknowledgements

This work was supported by the National Key Research and Development Program of China (2016YFA0203301), the National Natural Science Foundation of China (21773293 and U1710122), Jiangxi Provincial Natural Science Foundation (20202BAB204006), the Jiangxi Provincial Key Research and Development Project (20202BBEL53027), and the Natural Science Foundation of Jiangsu Province (BK20191196).

References

1 S. H. Wang, J. Xu, W. C. Wang, G. J. N. Wang, R. Rastak, F. Molina-Lopez, J. W. Chung, S. M. Niu, V. R. Feig, J. Lopez, T. Lei, S. K. Kwon, Y. Kim, A. M. Foudeh, A. Ehrlich, A. Gasperini, Y. Yun, B. Murmann, J. B. H. Tok and Z. A. Bao, *Nature*, 2018, **555**, 83–88.
2 W. Zeng, L. Shu, Q. Li, S. Chen, F. Wang and X. M. Tao, *Adv. Mater.*, 2014, **26**, 5310–5336.
3 M. Stoppa and A. Chiolerio, *Sensors*, 2014, **14**, 11957–11992.
4 Y. Liu, M. Pharr and G. A. Salvatore, *ACS Nano*, 2017, **11**, 9614–9635.
5 G. M. Zhou, F. Li and H. M. Cheng, *Energy Environ. Sci.*, 2014, **7**, 1307–1338.
6 X. F. Wang, X. H. Lu, B. Liu, D. Chen, Y. X. Tong and G. Z. Shen, *Adv. Mater.*, 2014, **26**, 4763–4782.
7 H. Wu, Y. A. Huang, F. Xu, Y. Q. Duan and Z. P. Yin, *Adv. Mater.*, 2016, **28**, 9881–9919.
8 B. J. Kim, D. H. Kim, Y. Y. Lee, H. W. Shin, G. S. Han, J. S. Hong, K. Mahmood, T. K. Ahn, Y. C. Joo, K. S. Hong, N. G. Park, S. Lee and H. S. Jung, *Energy Environ. Sci.*, 2015, **8**, 916–921.
9 G. X. Qu, J. L. Cheng, X. D. Li, D. M. Yuan, P. N. Chen, X. L. Chen, B. Wang and H. S. Peng, *Adv. Mater.*, 2016, **28**, 3646–3652.
10 Z. Wen, M. H. Yeh, H. Y. Guo, J. Wang, Y. L. Zi, W. D. Xu, J. N. Deng, L. Zhu, X. Wang, C. G. Hu, L. P. Zhu, X. H. Sun and Z. L. Wang, *Sci. Adv.*, 2016, **2**, 8.
11 F. N. Mo, G. J. Liang, Z. D. Huang, H. F. Li, D. H. Wang and C. Y. Zhi, *Adv. Mater.*, 2020, **32**, 1902151.
12 Z. Pan, J. Yang, J. Yang, Q. Zhang, H. Zhang, X. Li, Z. Kou, Y. Zhang, H. Chen, C. Yan and J. Wang, *ACS Nano*, 2020, **14**, 842–853.
13 Y. Jang, S. M. Kim, G. M. Spinks and S. J. Kim, *Adv. Mater.*, 2020, **32**, 1902670.
14 M. Zohair, K. Moyer, J. Eaves-Rathert, C. Meng, J. Waugh and C. L. Pint, *ACS Nano*, 2020, **14**, 2308–2315.
15 T. Lv, Y. Yao, N. Li and T. Chen, *Nano Today*, 2016, **11**, 644–660.
16 F. C. Meng, Q. W. Li and L. X. Zheng, *Energy Storage Mater.*, 2017, **8**, 85–109.
17 J. Di, X. Zhang, Z. Yong, Y. Zhang, D. Li, R. Li and Q. Li, *Adv. Mater.*, 2016, **28**, 10529–10538.
18 B. Vigolo, A. Penicaud, C. Coulon, C. Sauder, R. Pailler, C. Journet, P. Bernier and P. Poulin, *Science*, 2000, **290**, 1331–1334.
19 M. D. Lima, S. Fang, X. Lepro, C. Lewis, R. Ovalle-Robles, J. Carretero-Gonzalez, E. Castillo-Martinez, M. E. Kozlov, J. Oh, N. Rawat, C. S. Haines, M. H. Haque, V. Aare, S. Stoughton, A. A. Zakhidov and R. H. Baughman, *Science*, 2011, **331**, 51–55.
20 M. Zhang, K. R. Atkinson and R. H. Baughman, *Science*, 2004, **306**, 1358–1361.
21 X.-H. Zhong, Y.-L. Li, Y.-K. Liu, X.-H. Qiao, Y. Feng, J. Liang, J. Jin, L. Zhu, F. Hou and J.-Y. Li, *Adv. Mater.*, 2010, **22**, 692–696.

22 Y. Jung, Y. S. Cho, J. W. Lee, J. Y. Oh and C. R. Park, *Compos. Sci. Technol.*, 2018, **166**, 95–108.
23 Y. Bai, R. Zhang, X. Ye, Z. Zhu, H. Xie, B. Shen, D. Cai, B. Liu, C. Zhang, Z. Jia, S. Zhang, X. Li and F. Wei, *Nat. Nanotechnol.*, 2018, **13**, 589–595.
24 J. N. Wang, X. G. Luo, T. Wu and Y. Chen, *Nat. Commun.*, 2014, **5**, 3848.
25 J. Zhao, X. Zhang, J. Di, G. Xu, X. Yang, X. Liu, Z. Yong, M. Chen and Q. Li, *Small*, 2010, **6**, 2612–2617.
26 B. Aleman, V. Reguero, B. Mas and J. J. Vilatela, *ACS Nano*, 2015, **9**, 7392–7398.
27 J. Qiu, J. Terrones, J. J. Vilatela, M. E. Vickers, J. A. Elliott and A. H. Windle, *ACS Nano*, 2013, **7**, 8412–8422.
28 S. Li, X. Zhang, J. Zhao, F. Meng, G. Xu, Z. Yong, J. Jia, Z. Zhang and Q. Li, *Compos. Sci. Technol.*, 2012, **72**, 1402–1407.
29 K. Liu, Y. Sun, X. Lin, R. Zhou, J. Wang, S. Fan and K. Jiang, *ACS Nano*, 2010, **4**, 5827–5834.
30 M. Motta, Y. L. Li, I. Kinloch and A. Windle, *Nano Lett.*, 2005, **5**, 1529–1533.
31 S. Ryu, J. B. Chou, K. Lee, D. Lee, S. H. Hong, R. Zhao, H. Lee and S.-g. Kim, *Adv. Mater.*, 2015, **27**, 3250–3255.
32 F. Meng, X. Zhang, R. Li, J. Zhao, X. Xuan, X. Wang, J. Zou and Q. Li, *Adv. Mater.*, 2014, **26**, 2480–2485.
33 Y. Ye, X. Zhang, F. Meng, J. Zhao and Q. Li, *J. Mater. Chem. C*, 2013, **1**, 2009–2013.
34 F. Meng, J. Zhao, Y. Ye, X. Zhang and Q. Li, *Nanoscale*, 2012, **4**, 7464–7468.
35 S. Ryu, Y. Lee, J.-W. Hwang, S. Hong, C. Kim, T. G. Park, H. Lee and S. H. Hong, *Adv. Mater.*, 2011, **23**, 1971–1975.
36 A. Kis, G. Csanyi, J. P. Salvetat, T. N. Lee, E. Couteau, A. J. Kulik, W. Benoit, J. Brugger and L. Forro, *Nat. Mater.*, 2004, **3**, 153–157.
37 W. Xu, Y. Chen, H. Zhan and J. N. Wang, *Nano Lett.*, 2016, **16**, 946–952.
38 K. Koziol, J. Vilatela, A. Moisala, M. Motta, P. Cunniff, M. Sennett and A. Windle, *Science*, 2007, **318**, 1892–1895.
39 Q. Li, Y. Li, X. Zhang, S. B. Chikkannanavar, Y. Zhao, A. M. Dangelewicz, L. Zheng, S. K. Doorn, Q. Jia, D. E. Peterson, P. N. Arendt and Y. Zhu, *Adv. Mater.*, 2007, **19**, 3358–3363.
40 M. Salvato, M. Lucci, I. Ottaviani, M. Cirillo, E. Tamburri, I. Cianchetta, V. Guglielmotti, S. Orlanducci, M. L. Terranova and M. Pasquali, *Phys. Rev. B: Condens. Matter Mater. Phys.*, 2011, **84**, 233406.
41 T. Q. Tran, Z. Fan, P. Liu, S. M. Myint and H. M. Duong, *Carbon*, 2016, **99**, 407–415.
42 S. Liu, Y. Zhang, Y. Lin, Z. Zhao and Q. Li, *Carbon*, 2014, **69**, 247–254.
43 S. Luo, T. Liu, S. M. Benjamin and J. S. Brooks, *Langmuir*, 2013, **29**, 8694–8702.
44 M. Miao, J. McDonnell, L. Vuckovic and S. C. Hawkins, *Carbon*, 2010, **48**, 2802–2811.
45 P. Wang, D. Liu, J. Zou, Y. Ye, L. Hou, J. Zhao, C. Men, X. Zhang and Q. Li, *Mater. Des.*, 2018, **159**, 138–144.
46 N. Behabtu, C. C. Young, D. E. Tsentalovich, O. Kleinerman, X. Wang, A. W. K. Ma, E. A. Bengio, R. F. ter Waarbeek, J. J. de Jong, R. E. Hoogerwerf, S. B. Fairchild, J. B. Ferguson, B. Maruyama, J. Kono, Y. Talmon, Y. Cohen, M. J. Otto and M. Pasquali, *Science*, 2013, **339**, 182–186.
47 D. E. Tsentalovich, R. J. Headrick, F. Mirri, J. Hao, N. Behabtu, C. C. Young and M. Pasquali, *ACS Appl. Mater. Interfaces*, 2017, **9**, 36189–36198.
48 L. M. Ericson, H. Fan, H. Q. Peng, V. A. Davis, W. Zhou, J. Sulpizio, Y. H. Wang, R. Booker, J. Vavro, C. Guthy, A. N. G. Parra-Vasquez, M. J. Kim, S. Ramesh, R. K. Saini, C. Kittrell, G. Lavin, H. Schmidt, W. W. Adams, W. E. Billups, M. Pasquali, W. F. Hwang, R. H. Hauge, J. E. Fischer and R. E. Smalley, *Science*, 2004, **305**, 1447–1450.
49 V. A. Davis, A. N. G. Parra-Vasquez, M. J. Green, P. K. Rai, N. Behabtu, V. Prieto, R. D. Booker, J. Schmidt, E. Kesselman, W. Zhou, H. Fan, W. W. Adams, R. H. Hauge, J. E. Fischer, Y. Cohen, Y. Talmon, R. E. Smalley and M. Pasquali, *Nat. Nanotechnol.*, 2009, **4**, 830–834.
50 J. Zhao, Q. Li, B. Gao, X. Wang, J. Zou, S. Cong, X. Zhang, Z. Pan and Q. Li, *Carbon*, 2016, **101**, 114–119.
51 G. Xu, J. Zhao, S. Li, X. Zhang, Z. Yong and Q. Li, *Nanoscale*, 2011, **3**, 4215–4219.
52 R. E. A. Ardhi, M. X. Tran, M. Wang, G. Liu and J. K. Lee, *J. Mater. Chem. A*, 2020, **8**, 2549–2562.
53 H. Wang, Y. Liu, H. Huang, M. Zhong, H. Shen, Y. Wang and H. Yang, *Appl. Surf. Sci.*, 2009, **255**, 9020–9025.
54 Z. Lv, Y. Fu, S. Hou, D. Wang, H. Wu, C. Zhang, Z. Chu and D. Zou, *Phys. Chem. Chem. Phys.*, 2011, **13**, 10076–10083.
55 Z. Lv, J. Yu, H. Wu, J. Shang, D. Wang, S. Hou, Y. Fu, K. Wu and D. Zou, *Nanoscale*, 2012, **4**, 1248–1253.
56 M. M. Hossain, H. Shima, S. Son and J. R. Hahn, *RSC Adv.*, 2016, **6**, 71450–71460.
57 T. Chen, S. Wang, Z. Yang, Q. Feng, X. Sun, L. Li, Z. S. Wang and H. Peng, *Angew. Chem., Int. Ed. Engl.*, 2011, **50**, 1815–1819.
58 F. Cai, T. Chen and H. Peng, *J. Mater. Chem.*, 2012, **22**, 14856.
59 T. Chen, L. Qiu, Z. Cai, F. Gong, Z. Yang, Z. Wang and H. Peng, *Nano Lett.*, 2012, **12**, 2568–2572.
60 J. Yan, M. J. Uddin, T. J. Dickens, D. E. Daramola and O. I. Okoli, *Adv. Mater. Interfaces*, 2014, **1**, 1400075.
61 S. Zhang, C. Ji, Z. Bian, P. Yu, L. Zhang, D. Liu, E. Shi, Y. Shang, H. Peng, Q. Cheng, D. Wang, C. Huang and A. Cao, *ACS Nano*, 2012, **6**, 7191–7198.
62 S. Li, J. G. Park, Z. Liang, T. Siegrist, T. Liu, M. Zhang, Q. Cheng, B. Wang and C. Zhang, *Carbon*, 2012, **50**, 3859–3867.
63 X. Fang, Z. Yang, L. Qiu, H. Sun, S. Pan, J. Deng, Y. Luo and H. Peng, *Adv. Mater.*, 2014, **26**, 1694–1698.
64 H. Sun, X. You, J. Deng, X. Chen, Z. Yang, J. Ren and H. Peng, *Adv. Mater.*, 2014, **26**, 2868–2873.
65 T. Chen, L. Qiu, H. G. Kia, Z. Yang and H. Peng, *Adv. Mater.*, 2012, **24**, 4623–4628.
66 X. Fu, H. Sun, S. Xie, J. Zhang, Z. Pan, M. Liao, L. Xu, Z. Li, B. Wang, X. Sun and H. Peng, *J. Mater. Chem. A*, 2018, **6**, 45–51.

67 A. Ali, K. Shehzad, F. Ur-Rahman, S. M. Shah, M. Khurram, M. Mumtaz and R. U. Sagar, *ACS Appl. Mater. Interfaces*, 2016, **8**, 25353–25360.
68 Y. Jiang, H. Sun and H. Peng, *Sci. China Mater.*, 2015, **58**, 289–293.
69 Z. Yang, J. Deng, X. Sun, H. Li and H. Peng, *Adv. Mater.*, 2014, **26**, 2643–2647, 2613.
70 H. Sun, H. Li, X. You, Z. Yang, J. Deng, L. Qiu and H. Peng, *J. Mater. Chem. A*, 2014, **2**, 345–349.
71 S. Pan, Z. Yang, H. Li, L. Qiu, H. Sun and H. Peng, *J. Am. Chem. Soc.*, 2013, **135**, 10622–10625.
72 T. Chen, L. Qiu, H. Li and H. Peng, *J. Mater. Chem. A*, 2012, **22**, 23655.
73 Z. Zhang, Z. Yang, Z. Wu, G. Guan, S. Pan, Y. Zhang, H. Li, J. Deng, B. Sun and H. Peng, *Adv. Energy Mater.*, 2014, **4**, 1301750.
74 D. Liu, M. Zhao, Y. Li, Z. Bian, L. Zhang, Y. Shang, X. Xia, S. Zhang, D. Yun, Z. Liu, A. Cao and C. Huang, *ACS Nano*, 2012, **6**, 11027–11034.
75 B. Dong, J. Hu, X. Xiao, S. Tang, X. Gao, Z. Peng and D. Zou, *Adv. Mater. Technol.*, 2019, **4**, 1900131.
76 Q. Luo, H. Ma, Q. Hou, Y. Li, J. Ren, X. Dai, Z. Yao, Y. Zhou, L. Xiang, H. Du, H. He, N. Wang, K. Jiang, H. Lin, H. Zhang and Z. Guo, *Adv. Funct. Mater.*, 2018, **28**, 1706777.
77 L. Qiu, S. He, J. Yang, F. Jin, J. Deng, H. Sun, X. Cheng, G. Guan, X. Sun, H. Zhao and H. Peng, *J. Mater. Chem. A*, 2016, **4**, 10105–10109.
78 L. Qiu, S. He, J. Yang, J. Deng and H. Peng, *Small*, 2016, **12**, 2419–2424.
79 R. Li, X. Xiang, X. Tong, J. Zou and Q. Li, *Adv. Mater.*, 2015, **27**, 3831–3835.
80 J. Deng, L. Qiu, X. Lu, Z. Yang, G. Guan, Z. Zhang and H. Peng, *J. Mater. Chem. A*, 2015, **3**, 21070–21076.
81 G. Wang, S.-K. Kim, M. C. Wang, T. Zhai, S. Munukutla, G. S. Girolami, P. J. Sempsrott, S. Nam, P. V. Braun and J. W. Lyding, *ACS Nano*, 2020, **14**, 632–639.
82 Z. Pan, J. Zhong, Q. Zhang, J. Yang, Y. Qiu, X. Ding, K. Nie, H. Yuan, K. Feng, X. Wang, G. Xu, W. Li, Y. Yao, Q. Li, M. Liu and Y. Zhang, *Adv. Energy Mater.*, 2018, **8**, 1702946.
83 F. Zhu, W. Liu, Y. Liu and W. Shi, *Chem. Eng. J.*, 2020, **383**, 123150.
84 R. Xu, J. Wei, F. Guo, X. Cui, T. Zhang, H. Zhu, K. Wang and D. Wu, *RSC Adv.*, 2015, **5**, 22015–22021.
85 C. Choi, J. W. Park, K. J. Kim, D. W. Lee, M. J. de Andrade, S. H. Kim, S. Gambhir, G. M. Spinks, R. H. Baughman and S. J. Kim, *RSC Adv.*, 2018, **8**, 13112–13120.
86 B. Wang, X. Fang, H. Sun, S. He, J. Ren, Y. Zhang and H. Peng, *Adv. Mater.*, 2015, **27**, 7854–7860.
87 S. Pan, H. Lin, J. Deng, P. Chen, X. Chen, Z. Yang and H. Peng, *Adv. Energy Mater.*, 2015, **5**, 1401438.
88 Z. Lu, Y. Chao, Y. Ge, J. Foroughi, Y. Zhao, C. Wang, H. Long and G. G. Wallace, *Nanoscale*, 2017, **9**, 5063–5071.
89 J. Sun, Q. Zhang, X. Wang, J. Zhao, J. Guo, Z. Zhou, J. Zhang, P. Man, J. Sun, Q. Li and Y. Yao, *J. Mater. Chem. A*, 2017, **5**, 21153–21160.
90 J. Sun, P. Man, Q. Zhang, B. He, Z. Zhou, C. Li, X. Wang, J. Guo, J. Zhao, L. Xie, Q. Li, J. Sun, G. Hong and Y. Yao, *Appl. Surf. Sci.*, 2018, **447**, 795–801.
91 Z. Zhou, Q. Zhang, J. Sun, B. He, J. Guo, Q. Li, C. Li, L. Xie and Y. Yao, *ACS Nano*, 2018, **12**, 9333–9341.
92 J. Ren, L. Li, C. Chen, X. Chen, Z. Cai, L. Qiu, Y. Wang, X. Zhu and H. Peng, *Adv. Mater.*, 2013, **25**, 1155–1159.
93 P. Shi, L. Li, L. Hua, Q. Qian, P. Wang, J. Zhou, G. Sun and W. Huang, *ACS Nano*, 2017, **11**, 444–452.
94 G. Huang, Y. Zhang, L. Wang, P. Sheng and H. Peng, *Carbon*, 2017, **125**, 595–604.
95 Z. Niu, H. Dong, B. Zhu, J. Li, H. H. Hng, W. Zhou, X. Chen and S. Xie, *Adv. Mater.*, 2013, **25**, 1058–1064.
96 P. Man, Q. Zhang, J. Sun, J. Guo, X. Wang, Z. Zhou, B. He, Q. Li, L. Xie, J. Zhao, C. Li, Q. Li and Y. Yao, *Carbon*, 2018, **139**, 21–28.
97 Z. Cai, L. Li, J. Ren, L. Qiu, H. Lin and H. Peng, *J. Mater. Chem. A*, 2013, **1**, 258–261.
98 Q. Zhang, Z. Zhou, Z. Pan, J. Sun, B. He, Q. Li, T. Zhang, J. Zhao, L. Tang, Z. Zhang, L. Wei and Y. Yao, *Adv. Sci.*, 2018, **5**, 1801462.
99 J. Guo, Q. Zhang, J. Sun, C. Li, J. Zhao, Z. Zhou, B. He, X. Wang, P. Man, Q. Li, J. Zhang, L. Xie, M. Li and Y. Yao, *J. Power Sources*, 2018, **382**, 122–127.
100 Q. Zhang, W. Xu, J. Sun, Z. Pan, J. Zhao, X. Wang, J. Zhang, P. Man, J. Guo, Z. Zhou, B. He, Z. Zhang, Q. Li, Y. Zhang, L. Xu and Y. Yao, *Nano Lett.*, 2017, **17**, 7552–7560.
101 Q. Zong, Q. Zhang, X. Mei, Q. Li, Z. Zhou, D. Li, M. Chen, F. Shi, J. Sun, Y. Yao and Z. Zhang, *ACS Appl. Mater. Interfaces*, 2018, **10**, 37233–37241.
102 Q. Zhang, X. Wang, Z. Pan, J. Sun, J. Zhao, J. Zhang, C. Zhang, L. Tang, J. Luo, B. Song, Z. Zhang, W. Lu, Q. Li, Y. Zhang and Y. Yao, *Nano Lett.*, 2017, **17**, 2719–2726.
103 J. X. Zhao, L. L. Li, Y. Zhang, C. W. Li, Q. C. Zhang, J. H. Peng, X. X. Zhao, Q. L. Li, X. N. Wang, J. X. Xie, J. Sun, B. He, C. H. Lu, W. B. Lu, T. Zhang and Y. G. Yao, *Energy Storage Mater.*, 2018, **15**, 315–323.
104 C. Choi, J. M. Lee, S. H. Kim, S. J. Kim, J. Di and R. H. Baughman, *Nano Lett.*, 2016, **16**, 7677–7684.
105 C. Choi, K. M. Kim, K. J. Kim, X. Lepro, G. M. Spinks, R. H. Baughman and S. J. Kim, *Nat. Commun.*, 2016, **7**, 13811.
106 W. Son, S. Chun, J. M. Lee, Y. Lee, J. Park, D. Suh, D. W. Lee, H. Jung, Y. J. Kim, Y. Kim, S. M. Jeong, S. K. Lim and C. Choi, *Nat. Commun.*, 2019, **10**, 426.
107 S. Zeng, X. Tong, S. S. Zhou, B. Lv, J. Qiao, Y. H. Song, M. H. Chen, J. T. Di and Q. W. Li, *Small*, 2018, **14**, 9.
108 Y. Li, J. Zhou, T. Zhang, T. Wang, X. Li, Y. Jia, J. Cheng, Q. Guan, E. Liu, H. Peng and B. Wang, *Adv. Funct. Mater.*, 2019, **29**, 1808117.
109 J. Zhou, X. Li, C. Yang, Y. Li, K. Guo, J. Cheng, D. Yuan, C. Song, J. Lu and B. Wang, *Adv. Mater.*, 2019, **31**, 1903852.
110 Y.-H. Liu, H.-H. Lin, T.-Y. Tsai and C.-H. Hsu, *RSC Adv.*, 2019, **9**, 33117–33123.
111 Y. Zhang, Y. Wang, L. Wang, C.-M. Lo, Y. Zhao, Y. Jiao, G. Zheng and H. Peng, *J. Mater. Chem. A*, 2016, **4**, 9002–9008.
112 Y. Luo, Y. Zhang, Y. Zhao, X. Fang, J. Ren, W. Weng, Y. Jiang, H. Sun, B. Wang, X. Cheng and H. Peng, *J. Mater. Chem. A*, 2015, **3**, 17553–17557.

113 W. Weng, Q. Sun, Y. Zhang, H. Lin, J. Ren, X. Lu, M. Wang and H. Peng, *Nano Lett.*, 2014, **14**, 3432–3438.
114 J. Ren, Y. Zhang, W. Bai, X. Chen, Z. Zhang, X. Fang, W. Weng, Y. Wang and H. Peng, *Angew. Chem., Int. Ed. Engl.*, 2014, **53**, 7864–7869.
115 H. Lin, W. Weng, J. Ren, L. Qiu, Z. Zhang, P. Chen, X. Chen, J. Deng, Y. Wang and H. Peng, *Adv. Mater.*, 2014, **26**, 1217–1222.
116 C.-F. Sun, H. Zhu, E. B. Baker III, M. Okada, J. Wan, A. Ghemes, Y. Inoue, L. Hu and Y. Wang, *Nano Energy*, 2013, **2**, 987–994.
117 Y. Zhang, W. Bai, J. Ren, W. Weng, H. Lin, Z. Zhang and H. Peng, *J. Mater. Chem. A*, 2014, **2**, 11054.
118 X. Wang, Z. Pan, J. Yang, Z. Lyu, Y. Zhong, G. Zhou, Y. Qiu, Y. Zhang, J. Wang and W. Li, *Energy Storage Mater.*, 2019, **22**, 179–184.